Published in final edited form as:
J Phys Chem B. 2010 July 22; 114(28): 9259–9267. doi:10.1021/jp101448j.

Catalysis of Carboxypeptidase A: Promoted-water vs Nucleophilic Pathways

Shanshan Wu[1], **Chunchun Zhang**[2], **Dingguo Xu**[1,*], and **Hua Guo**[3,*]

[1]College of Chemistry, MOE Key Laboratory of Green Chemistry & Technology, Sichuan University, Chengdu, Sichuan 610064, P. R. China

[2]Analytical & Testing Center, Sichuan University, Chengdu, Sichuan 610064, P.R. China

[3]Department of Chemistry and Chemical Biology, University of New Mexico, Albuquerque, New Mexico 87131, USA

Abstract

The catalytic mechanism of carboxypeptidase A (CPA) for the hydrolysis of ester substrates is investigated using hybrid quantum mechanical/molecular mechanical (QM/MM) methods and high-level density functional theory. The prevailing mechanism was found to utilize an active-site water molecule assisted by Glu270 and this so-called promoted-water pathway is similar to that in the CPA catalyzed proteolytic reaction (D. Xu and H. Guo, J. Am. Chem. Soc. 131, 9780 (2009)). On the other hand, our simulations indicated the existence of an alternative pathway due to direct nucleophilic attack of Glu270 on the scissile carbonyl carbon. This so-called nucleophilic pathway, which is not viable in proteolytic reactions, leads to a stable acyl-enzyme complex. However, the nucleophilic pathway is non-productive as it is blocked by a high barrier in the deacylation step. Based on results reported here and in our earlier publication, a unified model is proposed to account for nearly all experimental observations concerning the catalysis of CPA.

1. Introduction

Carboxypeptidase A (CPA, EC 3.4.17.1) is a monozinc exopeptidase from the pancreas, specializing in the elimination of a hydrophobic C-terminal amino acid by cleaving the backbone amide bond.1 In addition to its natural substrates, CPA also hydrolyzes esters with similar configurations, often with faster rates. Being arguably the most extensively studied zinc hydrolases,2⁻4 CPA was one of the first proteins whose high-resolution structures were ever determined by X-ray diffraction.5 Since then, numerous additional structures of CPA complexed with inhibitors, substrate analogs, and transition-state analogs have been determined,6⁻21 which has shed much light on the mode of catalysis of CPA and other related zinc hydrolases. It is now well established that the obligatory divalent zinc cofactor is coordinated by three protein ligands (His69, Glu72, and His196). The fourth ligand is a water molecule in the apo enzyme, but its identity is less established in the Michaelis complex. In the second shell, there are several key residues including Glu270, Arg127, Tyr248, Arg71, Asn144, and Arg145 and mutagenesis studies have helped to elucidate the roles of these residues.22⁻26 The ample structural information about CPA has greatly

*Corresponding authors, dgxu@scu.edu.cn (DX) and hguo@unm.edu (HG).

Supporting Information: Geometry of the DFT stationary points and key internuclear distances for both the promoted-water and nucleophilic pathways, as well as the full citations for Refs. 57 and 85. This material is available free of charge via the internet at http://pubs.acs.org.

benefited the search for inhibitors of zinc peptidases of medicinal importance, such as the angiotensin-converting enzyme (ACE),27 which regulates blood pressure.

Despite the rich experimental data, the catalytic mechanism of CPA still remains controversial.3–4, 28–30 Two major pathways have been proposed, as depicted in Scheme 1. The so-called promoted-water (or general base-general acid) pathway assigns Glu270 with a dual role. In the initial nucleophilic addition step, it serves as a general base to facilitate the attack of the zinc-bound water at the scissile carbonyl carbon by transferring a water proton to a carboxylate oxygen. In the second elimination step, it acts as a general acid to transfer this proton to the leaving nitrogen group. The alternative nucleophilic or "anhydride" mechanism, on the other hand, envisages a direct nucleophilic attack by the carboxylate side chain of Glu270 at the scissile carbonyl carbon, necessitating an acyl-enzyme intermediate, which can be eventually hydrolyzed by water.

The promoted-water mechanism is consistent with most X-ray structures and kinetic data. In addition, Breslow and Wernick have concluded from their ^{18}O isotope labeling experiments that the acyl-enzyme complex is unlikely to exist for peptide substrates.30–31 However, several authors have reported the detection of intermediates for ester substrates at low temperatures.32–36 Although these intermediates were not definitively characterized, they were believed to be the sought-after acyl-enzyme complex and taken as evidence in support of the nucleophilic mechanism. Some of the interpretations of the experimental observations were later questioned by others,3, 37–38 but more definitive data were presented subsequently in support of the existence of the acyl-enzyme intermediate in esterolysis.39–41

These seemingly conflicting experimental data could be reconciled by assuming that the proteolytic and esterolytic reactions favor different mechanisms.30 This idea has indeed some experimental support. Vallee and coworkers have for example found that the catalyzed hydrolysis of two types of substrates has rather different binding and kinetic behaviors.38, 42–44 X-ray structures also indicate that esters typically bind with direct metal coordination by the scissile carbonyl, while such an interaction is considered non-productive for the peptides.3 On the other hand, Cleland speculated that the two reactions may have the same mechanism, but with different rate-limiting steps.2 However, little experimental support for this hypothesis has been found so far.

Given the experimental difficulties in distinguishing the two mechanisms, it is desirable to address these issues theoretically. Earlier studies have been limited to quantum chemical models45–49 or molecular dynamics (MD) studies,50 which either ignored the protein environment or provided no information on the reaction. More recently, the CPA catalysis has been investigated by several groups using hybrid quantum mechanical and molecular mechanical (QM/MM) methods.51–53 For example, we have reported an extensive theoretical investigation of the CPA catalysis using both a QM/MM method and density functional theory.53 This study focused on the proteolytic reaction and found that the promoted-water mechanism is consistent with structural, kinetic, and mutagenesis data. The same conclusion was also reached in an independent QM/MM investigation by Klishtain and Warshel.52

Our recent work also explored the nucleophilic pathway and found it is not viable for the peptide substrate.53 Detailed analysis of the active-site structure attributed the failure to the poor alignment of the reactants, the weak nucleophilicity of the carboxylate, and perhaps most importantly a hydrogen bond formed between the substrate amide group and Glu270 carboxylate, which further reduces its nucleophilicity. Interestingly, the latter feature is absent in CPA catalyzed esterolytic reactions where the backbone N-C bond of the substrate

is replaced by an O-C bond, suggesting that the nucleophilic pathway might be viable for ester substrates. In this work, we present our theoretical analysis of the ester hydrolysis reaction catalyzed by CPA, which allows us to rationalize the existing experimental observations and to offer a holistic perspective on the multifaceted catalytic mechanism of this prototypical enzyme.

2. Methods

2.1 QM/MM models

Hybrid quantum mechanical and molecular mechanical (QM/MM) approach54 has been widely used to investigate enzymatic reaction mechanisms. (For a recent review see Ref. 55) The premise of the QM/MM scheme is to divide the system into two parts: the smaller QM region where the chemical bond breaking and forming take place is treated with quantum mechanics, while the surrounding region can be sufficiently described by a MM force field. As a result, large systems such as enzymes can be handled efficiently with reasonable accuracy.

In most calculations reported here, the QM region is treated with the self-consistent charge-density functional tight binding (SCC-DFTB) model56 while the MM region by the CHARMM all atom force field.57 The SCC-DFTB method is an approximate DFT method and thus much more efficient than ab initio QM/MM approaches. The efficiency is essential for metallo-enzymes because the active site is often much too large for accurate ab initio QM/MM free-energy simulations, perhaps with a few exceptions.58–59 The SCC-DFTB model has been extensively tested for enzyme systems,60–64 including active sites with zinc cofactors.65 In particular, the SCC-DFTB/CHARMM approach has been shown to give a satisfactory description of several zinc enzymes including carbonic anhydrase66–67 and β-lactamases.68–72 For instance, the free-energy barrier of for the CphA-catalyzed hydrolysis of biapenem obtained by the same SCC-DFTB/CHARMM approach69 has recently been accurately reproduced by a hybrid Car-Parrinello QM/MM study.73

To further confirm the accuracy of the SCC-DFTB/MM model, we have performed single point calculations at the B3LYP/MM level along the reaction paths determined by the SCC-DFTB/MM Hamiltonian for the nucleophilic pathway. For the QM region, the standard 6-31G(d) basis set was used for C, H, O and N atoms, while the Lanl2DZ ECP basis set for the zinc ion. Despite its accuracy, such high-level QM/MM approach is too expensive computationally to obtain PMFs in systems studied here. These calculations were carried out using a GAMESS-UK/CHARMM interface.

The model for CPA was adapted from our recent work on the hydrolysis of hippuryl-$_{L}$-Phe (HPA).53 The coordinates were modified from the X-ray structure of the wild-type (WT) bovine CPA complexed with the ZAA^{P}(O)F inhibitor (PDB code 6CPA).16 To study the catalyzed esterolytic reaction, the peptide substrate (HPA) was replaced by the corresponding ester, hippuryl-$_{D,L}$-β-phenyllactate (HPL) (Scheme 2A), which facilitates a direct comparison with the CPA-catalyzed proteolytic reaction studied earlier.53 Using the same setup protocol, the system was first solvated repeatedly using a rotating pre-equilibrated TIP3P74 water sphere with a 25Å radius centered at the zinc ion. Stochastic boundary conditions75 were enforced to reduce computation costs. In particular, the system was divided into three layers: atoms within the inner reaction zone (r < 22Å) were treated with Newtonian dynamics. Atoms in the buffer zone (22Å< r < 25Å) were treated using Langevin dynamics. Those atoms in the reservoir zone (r > 25Å) were removed. The link atom approach76 was employed to cover the covalent interface between the QM and MM regions. A group-based switching scheme was used for non-bonded interactions.77 All simulations were performed with the CHARMM suite of simulation codes.78

For the promoted-water mechanism (Scheme 2A), the QM region includes the entire HPL molecule, the zinc ion, the zinc-bound water, and side chain atoms of His69, Glu72, His196, Arg127 and Glu270. For the nucleophilic pathway, the zinc-bound water was removed and its coordination with the zinc ion was replaced by the scissile carbonyl oxygen (O_7). (In principle, the zinc-bound water could be present for the nucleophilic pathway, but our tests showed that the barrier is exceedingly high. As a result, this scenario is not considered here.) Except for the absence of the water molecule, the labeling scheme is identical to that in Scheme 2A. In the subsequent deacylation step, a nearby MM water molecule was re-introduced into the QM region to serve as the nucleophile, as shown in Scheme 2B, and it is located between Glu270 side chain group and the HPL molecule.

Both models were subjected to 1.0 ns QM/MM molecular dynamics (MD) simulations to investigate the stability of the enzyme-substrate (ES) complex. The systems were first brought from 0 K to 300 K in 30 ps, and allowed to equilibrate in the next 270 ps. The subsequent 700 ps MD trajectories were used for data analysis. For the nucleophilic pathway, the position of the added water for the second hydrolysis step has a large impact on the reaction barrier. Hence, we also performed a 700 ps MD simulation for the acyl-enzyme intermediate, with 200 ps equilibration. The integration step for all of MD simulations was 1.0 fs, and the SHAKE algorithm79 was applied to maintain all covalent bonds involved hydrogen atoms.

To examine the two mechanisms, snapshots were taken from the MD trajectories as the initial structures for reaction path calculations after minimization. Subsequently, these structures are driven along the respective reaction coordinate via adiabatic mapping. For the promoted-water mechanism, the reaction coordinate for the nucleophilic addition (NA) step was defined by the distance between the water oxygen atom (O_w) and the scissile carbonyl carbon atom (C_6): $r_1 = d_{O_w \cdots C_6}$. The corresponding reaction coordinate for the elimination (E) of the leaving group was given by the distance between C_6 atom and the ester oxygen atom (O_9), $r_2 = d_{O_9 \cdots C_6}$. For the nucleophilic pathway, the reaction coordinate for the acylation (A) step was defined as $r_1' = d_{C_6 \cdots O_{\varepsilon 2}(E270)}$; the reaction coordinate for the deacylation (DA) of the acyl-enzyme intermediate is given by the distance between the oxygen atom (O_w) of the added water molecule and the carboxylate carbon (C_{TM}) of Glu270, $r_2' = d_{O_w \cdots C_\delta(E270)}$.

Potentials of mean force (PMFs) for both mechanisms were computed using umbrella sampling80 with the reaction paths as initial structures. The harmonic force constant used here ranged from 100 to 150 kcal/mol·Å^2. In each window, 60 ps equilibration simulations were first performed to bring the system to 300K. The distribution function in the reaction coordinate was then collected in the subsequent 40 ps. The final PMF was obtained using the weighted histogram analysis method (WHAM).81 For the NA and E steps of promoted-water pathway, 11 and 13 windows were used, respectively. For the nucleophilic pathway, 13 and 11 windows were used for A and DA steps, respectively.

2.2 Truncated active-site models

To provide an independent check on the QM/MM calculations, we have also examined the reaction mechanisms using high-level density functional theory (DFT), but with truncated active-site models. These models are slightly different for the two mechanisms. For the promoted-water mechanism, it consists of the zinc ion, analogs of its three protein ligands and Glu270, an analog of the substrate, side chain groups of Arg127 and Arg145 to simulate the substrate binding environment. For the nucleophilic mechanism, on the other hand, there are two models. The first model leading to the acyl-enzyme complex is essentially the same as that for the promoted-water model, minus the water nucleophile. For the hydrolysis of the

acyl-enzyme, an additional water molecule was introduced between the substrate and Glu270 in the second model, as in the QM/MM calculations.

All stationary points were fully optimized without any constraint. Harmonic frequency calculations were then performed to confirm the minima and transition states. Intrinsic reaction coordinate (IRC) calculations82 were also carried out to connect the relevant stationary points. In this work, the hybrid B3LYP exchange-correlation functional83–84 and a standard 6-31G(d) basis set were used for all calculations. The solvent effects were included using the polarized continuum model (PCM)82 with either the water (ε=80) or protein (ε=5) environment, respectively. All calculations were carried out using the Gaussian03 suite of electronic structure programs.85

3. Results

3.1 Promoted-water pathway

A. Enzyme-substrate complex—The ES complex in the promoted-water pathway is quite stable in the 1.0 ns SCC-DFTB/MM MD simulation, as evidenced by the root mean square deviation (RMSD) for the backbone atoms displayed in Fig. 1. It is stabilized after the first 300 ps of equilibration and the averaged RMSD for the later 700 ps is 0.70±0.04 Å. A snapshot extracted from the MD simulation is given in Fig. 2A, and some selected key internuclear distances are listed in Table 1.

Throughout the simulation, the zinc ion maintains its tetra-coordination with His69, His196, Glu72, and the water molecule. The zinc bound water is well positioned for attacking the scissile carbonyl carbon (C_6), with a O_w-C_6 distance of 3.39±0.24 Å. The near attack position of the water is maintained by two hydrogen bonds, provided by the Glu270 side chain ($d_{H_1 \cdots O_{\varepsilon 2}(E270)}$ = 1.45±0.13Å) and Ser197 backbone oxygen ($d_{H_2 \cdots O(S197)}$ = 1.75±0.19 Å). The scissile carbonyl oxygen (O_7), on the other hand, has no direct contact with Zn(II). This arrangement is very similar to that in the ES complex with HPA.53

The substrate interacts with the enzyme via a network of hydrogen bonds. For example, the substrate C-terminal carboxylate group (O_{12} and O_{13}) are anchored by the Arg127, Asn144, Arg145 and Tyr248 side chains groups. The benzoyl carbonyl oxygen of the hippruyl group is also hydrogen bonded with side chain groups of Arg71 and Arg127, respectively. In addition, Arg127 can form relatively weak hydrogen bonds with the scissile carbonyl oxygen (O_7), as in the CPA-HPA complex studied earlier.53

B. PMF—As in our previous work,53 the promoted-water pathway consists of two steps. In the first NA step, the zinc-bound water nucleophile, assisted by the Glu270 general base, attacks the scissile carbonyl carbon, resulting in a tetrahedral intermediate (TI). In the second E step, the protonation of the nitrogen leaving group leads to the cleavage of peptide bond and thus the enzyme-product (EP) complex. The calculated PMFs for the two steps are displayed in Fig. 3, which shows the TI flanked by two transition states (TS1 and TS2). The corresponding ES, TS1, TI, TS2, and EP structures are shown in Fig. 4, and some key geometric parameters are listed in Table 1 as well. These structures indicate that the scissile carbonyl in the ES complex is polarized by Arg127, which along with the zinc ion, serves as the “oxyanion hole” to stabilize the fractional charge developed on the carbonyl oxygen (O_7) upon the attack of the hydroxide nucleophile. As in the proteolytic reaction, Glu270 serves as the general base and general acid in the NA and E steps, respectively.

The calculated free energy barrier for the initial rate-limiting NA step is 12.7 kcal/mol, while that for the second E step is 5.7 kcal/mol. The overall barrier height is in excellent agreement with the experimental value of 13.3 kcal/mol (estimated from the k_{cat}=1197 s^{-1}

for a similar ester substrate Bz-Gly-OPhe)),22 and approximately 5.2 kcal/mol lower than that calculated for the CPA-catalyzed hydrolysis of HPA.53 The lower barrier for esterolytic reaction is a well-known effect, underscoring the fact that extra energy is needed to break the conjugated carboxamide (HN-CO) system in peptides.2 These results suggest that the promoted-water pathway is also viable for ester substrates, as for peptide substrates.

C. Truncated active-site model—The viability of the promoted-water pathway for the ester substrate was confirmed by the truncated active-site model at the B3LYP/6-31G(d) level of theory. As in the proteolytic reaction,53 six stationary points (ES, TS1, TI1, TI2, TS3, and EP) have been identified, and two corresponding to transition states (TS1 and TS3) for the NA and E steps, respectively. Despite many attempts, the transition state between TI1 and TI2 could not be located. However, this barrier is conformational in nature and is not expected to be significant.53 The structures and selected key geometrical parameters of these stationary points can be found in Supporting Information (SI), and they are very similar to the active-site arrangement obtained in the QM/MM calculations.

As shown in Table 2, the DFT energy barriers are 24.4 and 9.23 kcal/mol for the NA and E steps, respectively. The dominance of the first barrier is consistent with our QM/MM results. The higher barrier observed in the truncated active-site model is presumably due to the lack of the enzymatic environment. Indeed, a significant solvent effect is seen in Table 2 to lower the barrier. Single point calculations at a high level of theory (B3LYP/6-31+G(d,p)) did not change the qualitative features of the reaction. In addition, SCC-DFTB single point calculations at the B3LYP optimized geometries yielded energies that are close to those at the B3LYP level of theory, which further affirms the validity of SCC-DFTB in the QM/MM simulations.

2. Nucleophilic pathway

A. Enzyme-substrate complex—The 1.0 ns MD simulation for the ES complex for the nucleophilic pathway yielded a backbone RMSD of 0.72±0.03Å, as shown in the Fig. 1. Selected geometrical properties of the ES complex are listed in Table 3 and a snapshot from the MD trajectory is displayed in Fig. 2B. Different from the ES structure for the promoted-water mechanism, the substrate carbonyl binds directly to the zinc ion with a O_7-Zn distance of 2.17±0.08 Å. The direct zinc coordination allows the polarization of the carbonyl, making it more susceptible to nucleophilic attack. In the absence of the zinc-bound water, the Glu270 nucleophile is in a near attack position with $d_{O_{\varepsilon 2} \cdots C_6}$ = 3.32±0.17Å.

Another major difference between the CPA-HPA and CPA-HPL complexes is the interaction between the carboxylate side chain of Glu270 and the substrate. In the former, a hydrogen bond is formed between the backbone NH group and $O_{\varepsilon 1}$, while no such interaction exists for HPL substrate because the NH group is replaced by an O atom. Instead, there is slight repulsion between the two, as evidenced by the distance between O_9 and $O_{\varepsilon 1}$ of 3.40±0.33 Å. Furthermore, the carboxylate nucleophile and the substrate carbonyl are much better aligned in the CPA-HPL complex. The $O_{\varepsilon 2}$(E270)-C_6-O_7 angle in the CPA-ester complex is ~107°, close to a perpendicular (90°) approach, while the corresponding angle for the CPA-peptide complex is ~142°.

The remainder of the enzyme-substrate interaction is similar. For example, at the substrate C-terminal, the carboxylate group is hydrogen bonded with Arg127, Asn144, Arg145 and Tyr248 as well. The benzoyl carbonyl oxygen of hippuryl group is also anchored by Arg127 and Arg71 side chain groups. A difference from the promoted-water ES complex is the absence of the hydrogen bond between Arg127 and the scissile carbonyl oxygen (O_7) atom, as this oxygen atom has become the fourth ligand of the zinc ion.

B. Acyl-enzyme intermediate—To gain further insights into the nucleophilic pathway, we have performed MD simulations for the acyl-enzyme (AE) intermediate with the SCC-DFTB/CHARMM Hamilotonian. Throughout the 700 ps simulation, the acyl-enzyme complex is stable, judging from the $d_{C_6 \cdots O_{\varepsilon 2}(E270)}$ distance of 1.40±0.06 Å. The hydrolysis of the acyl-enzyme complex requires a water molecule in the active site. Indeed, a water molecule was identified in the MD simulation, which forms a stable hydrogen bond with Glu270 with a distance of $d_{H_1 \cdots O_{\varepsilon 1}(E270)}$ is 1.83±0.28 Å). A snapshot of the active site is displayed in Fig. 5.

C. Potentials of Mean Force—As shown by the PMFs in Fig. 6, the nucleophilic addition of the Glu270 carboxylate to the scissile carbonyl carbon (the acylation or A step) has a free energy barrier of only 2.6 kcal/mol, leading to a stable acyl-enzyme complex with a depth of 6.4 kcal/mol. This is in sharp contrast to the proteolytic reaction, in which the nucleophilic attack of Glu270 results in no stable acyl-enzyme complex.53 On the other hand, the deacylation or DA step, which features the nucleophilic attack of the water to the Glu270 carboxylate carbon, has a significant barrier of 18.7 kcal/mol. As a result, the nucleophilic pathway is limited by the deacylation step, and the barrier is about 5.4 kcal/mol higher than the experimental value of 13.3 kcal/mol.22 The stationary states for the ES, TS1, AE1, AE2, TS2 and EP are displayed in Fig. 7, and selected key geometrical parameters are listed in Table 3.

It should be noted here that our model (see Scheme 1) assumes the DA step is initiated by the attack of the water nucleophile to the Glu270 carboxylate carbon, which is in a sp^2 plane. It is thus different from the anhydride mechanism proposed earlier for the proteolytic reaction,49 in which the nucleophilic attack of OH^- occurs at the sp^3 hybridized C_6 in the acyl-enzyme complex, preceded by proton transfer to the nitrogen leaving group and the cleavage of the amide bond. According to our calculations (not shown here), the energy costs are too high for the latter scenario. This is consistent with the results reported in Ref. 49, in which the protonation step has an extremely high (48.2 kcal/mol) barrier. This observation indicates that the anhydride intermediate is irrelevant for the CPA catalysis, and the historical notion of the “anhydride” pathway is a misnomer.

D. Single-point B3LYP/MM calculations—To ascertain the reliability of the PMFs obtained at the SCC-DFTB/MM level of theory, we have computed single-point energies along the reaction paths determined by the SCC-DFTB/CHARMM Hamiltonian. The results, shown in Fig. 6 as filled circles, are in qualitative agreement with the PMFs. In other words, the higher level theory confirmed the low barrier for the formation of the acyl-enzyme complex, the stability of the acyl-enzyme intermediate, and the high barrier for the deacylation step. Note here that quantitative agreement between the two is not expected because no fluctuation was included in the single-point calculations.

E. Truncated active-site model—In our previous work,53 the DFT results for the first (A) step of the nucleophilic pathway have been reported with a smaller model. The calculations have now been repeated with a model comparable to that used for the promoted-water pathway. To simulate the DA step, we have introduced a water molecule into the truncated active-site model. Like in the QM/MM model, this water is hydrogen bonded to the Glu270 carboxylate group. The calculated energetics of the stationary points is given in Table 4 and their structures and several important internuclear distances can be found in SI.

As in our earlier report, the active-site model revealed that a stable acyl-enzyme complex exists. The DFT barrier height (TS1) for the A step is 16.61 kcal/mol, but it is sensitive to the environment as indicated the dramatic decrease of barrier and the energy of the acyl

intermediate (AE1) in polar solvent. The barrier for the DA step is 35.02 kcal/mol. The high barrier in the second DA step is consistent with the QM/MM results, indicating an improbable role for the nucleophilic pathway in the hydrolysis reaction.

4. Discussion

Despite the accumulation of experimental data, the catalytic mechanism of CPA is still under debate. A comprehensive theoretical study, such as the one reported here, provides a complementary perspective and microscopic insights. Our results reported here and earlier53 paint an interesting picture for CPA catalysis. For proteolytic reactions catalyzed by CPA, unequivocal evidence from our earlier simulations53 suggests that the promoted-water pathway is the sole viable mechanism. The situation for esterolytic reactions is, on the other hand, quite different. According to free-energy simulations reported here, both the promoted-water and nucleophilic pathways are viable, but the former has a much lower overall barrier. As a result, the promoted-water pathway would be preferred under normal reaction conditions. However, at low temperatures, the first step of the nucleophilic pathway, namely the formation of a stable acyl-enzyme complex, can compete effectively with the promoted-water pathway. This explains the numerous experimental observations of a trapped acyl-enzyme complex in CPA catalyzed esterolytic reactions. Despite this observation, our results do not lend support to the nucleophilic mechanism, because the second deacylation barrier is too high comparing with both experiment data and the calculated barrier for the promoted-water pathway. It is conceivable that the trapped acyl-enzyme complex eventually reverts to the ES complex, given the relative small barrier for the process (9.0 kcal/mol) and the reaction ultimately takes place via the promoted-water pathway after a water molecule enters the active site between the Zn cofactor and Glu270. It should be noted that the active-sites with and without the zinc-bound water represent different thermodynamic states and the free-energy between the two is unknown, but probably small. This proposed catalytic mechanism is illustrated in Fig. 8.

Our results further suggest that the availability of the nucleophilic pathway in esterolytic reactions is likely due to the absence of the hydrogen bond between the amide NH group in peptide substrate and the nucleophilic carboxylate of Glu270. In addition, the ester O-C bond can freely rotate while the N-C bond is much more rigid due to delocalization of the π orbital in the planar amino carbonyl group. As a result, the attacking carboxylate nucleophile can readily access the π^* orbital in ester substrates, but might have difficulties for peptide substrates.

Our conclusion that the prevalent mechanism for both proteolysis and esterolysis does not involve an acyl-enzyme intermediate is consistent with that reached by Vallee and coworkers.38, 44 It should be noted that our proposed mechanism differs conceptually from either Breslow's speculation that the two reactions have different mechanisms,30 or Cleland's proposal that the two reactions may have the same mechanism but different rate-limiting steps.2 However, there are some common components. For example, Breslow's proposal speculated that the nucleophilic pathway is only open for ester substrate, which is consistent with our observation of the acyl-intermediate reported here. On the other hand, Cleland's suggestion that both reactions proceed via the same pathway is in agreement with our evidence presented here.

This unified picture seems to reconcile almost all experimental observations on CPA catalysis. Perhaps the only exception is the hydrolysis of the dipeptide glycyl-L-tyrosine, where an acyl-enzyme complex was detected by Lee et al. at a low temperature.41 This is a special case as k_{cat} for this reaction is exceptional small86 and the X-ray structure of the ES complex indicated direct carbonyl coordination to the zinc ion and the absence of water in

the active site.13 In addition, this observation has not been confirmed with any other peptide substrate. Studies are underway in our labs and the results will be reported in a future publication.

5. Conclusions

In this work, we have investigated the catalytic mechanisms of a prototypical zinc peptidase (CPA) using hybrid QM/MM methods and density functional theory. The results revealed that the catalytic reactions for peptide and ester substrates can be quite different. While the proteolytic reaction proceeds exclusively via the promoted-water pathway, the esterolytic reaction can visit an acyl-enzyme intermediate along the nucleophilic pathway. This observation explains the numerous experimental observations of a trapped intermediate with ester substrates. However, our simulation results do not support the nucleophilic pathway as the barrier in the second deacylation step is significantly higher than that required by the promoted-water pathway. This unified model seems to reconcile with most experimental observations in both proteolytic and esterolytic reactions catalyzed by CPA.

Supplementary Material

Refer to Web version on PubMed Central for supplementary material.

Acknowledgments

This work was supported by SRF for ROCS, SEM and Chinese National Natural Science Foundation of China (No. 20803048 to DX) and by NIH (R03-AI071992 to HG). Some of the calculations have been performed at the National Center for Supercomputing Applications (NCSA).

References

1. Vallee, BL.; Galdes, A.; Auld, DS.; Riordan, JF. Carboxypeptidase A. In: Spiro, TG., editor. Zinc Enzymes. 1983.
2. Cleland WW. Adv. Enzymol. Relat. Areas Mol. Biol. 1977; 45:273–387. [PubMed: 21524]
3. Christianson DW, Lipscomb WN. Acc. Chem. Res. 1989; 22:62–69.
4. Lipscomb WM, Strater N. Chem. Rev. 1996; 96:2375–2433. [PubMed: 11848831]
5. Reeke GN, Hartsuck JA, Ludwig ML, Quiocho FA, Steitz TA, Lipscomb WN. Proc. Nat. Acad. Sci. 1967; 58:2220–2226. [PubMed: 16591584]
6. Rees DC, Lipscomb WN. J. Mole. Biol. 1982; 160:475–498.
7. Rees DC, Lipscomb WN. Proc. Natl. Acad. Sci. 1983; 80:7151–7154. [PubMed: 6580631]
8. Rees DC, Lipscomb WN. J. Mole. Biol. 1983; 168:367–387.
9. Christianson DW, Lipscomb WN. Proc. Natl. Acad. Sci. 1985; 82:6840–6844. [PubMed: 3863130]
10. Christianson DW, Kuo LC, Lipscomb WN. J. Am. Chem. Soc. 1985; 107:8281–8283.
11. Christianson DW, Lipscomb WN. J. Am. Chem. Soc. 1986; 108:545–546.
12. Christianson DW, Lipscomb WN. J. Am. Chem. Soc. 1986; 108:4998–5003.
13. Christianson DW, Lipscomb WN. Proc. Natl. Acad. Sci. 1986; 83:7568–7572. [PubMed: 3463986]
14. Christianson DW, Lipscomb WN. J. Am. Chem. Soc. 1987; 109:5536–5538.
15. Christianson DW, Lipscomb WN. J. Am. Chem. Soc. 1988; 110:5560–5565.
16. Kim H, Lipscomb WN. Biochem. 1990; 29:5546–5555. [PubMed: 2386784]
17. Mangani S, Carloni P, Orioli P. J. Mole. Biol. 1992; 223:573–578.
18. Teplyakov A, Wilson KS. Acta Cryst. 1993; D49:534–540.
19. Greenblatt HM, Feinberg H, Tucker PA, Shoham G. Acta Cryst. 1998; D54:289–305.
20. Cho JH, Kim DH, Chung SJ, Ha N-C, Oh B-H, Choi KY. Bioorg. Med. Chem. 2002; 10:2015–2022. [PubMed: 11937361]

21. Kilshtain-Vardi A, Glick M, Greenblatt HM, Goldblum A, Shoham G. Acta Cryst. 2003; D59:323–333.
22. Gardell SJ, Craik CS, Hilvert D, Urdea MS, Rutter WJ. Nature. 1985; 317:551–555. [PubMed: 3840231]
23. Hilvert D, Gardell SJ, Rutter WJ, Kaiser ET. J. Am. Chem. Soc. 1986; 108:5298–5304.
24. Phillips MA, Fletterick R, Rutter WJ. J. Biol. Chem. 1990; 265(33):20692–20698. [PubMed: 2243116]
25. Phillips MA, Rutter WJ. Protein Sci. 1992; 1:517–521. [PubMed: 1304353]
26. Cho JH, Kim DH, Kim D-H, Lee KJ, Choi KY. Biochem. 2001; 40:10197–10203. [PubMed: 11513597]
27. Ondetti MA, Cushman DW. Annu. Rev. Biochem. 1982; 51:283. [PubMed: 6287916]
28. Mock WL, Zhang JZ. J. Biol. Chem. 1991; 266:6393–6400. [PubMed: 2007591]
29. Fersht, AR. Enzyme Structure and Mechanism in Protein Science. New York: Freeman; 1999.
30. Breslow R, Wernick DL. Proc. Nat. Acad. Sci. 1977; 74:1303–1307. [PubMed: 266172]
31. Breslow R, Wernick DL. J. Am. Chem. Soc. 1976; 98:259–261. [PubMed: 1244372]
32. Makinen MW, Kuo LC, Dymowski JJ, Jaffer S. J. Biol. Chem. 1979; 254(2):356–366. [PubMed: 33168]
33. Makinen MW, Fukuyama JM, Kuo LC. J. Am. Chem. Soc. 1982; 104:2667–2669.
34. Kuo LC, Makinen MW. J. Biol. Chem. 1982; 257:24–27. [PubMed: 6273427]
35. Suh J, Cho W, Chung S. J. Am. Chem. Soc. 1985; 107:4530–4535.
36. Sander ME, Witzel H. Biochem. Biophys. Res. Commun. 1985; 132:681. [PubMed: 4062944]
37. Hoffman SJ, Chu SS-T, Lee H-H, Kaiser ET, Carey PR. J. Am. Chem. Soc. 1983; 105:6971–6973.
38. Auld DS, Galdes A, Geoghegan KF, Holmquit B, Martinelli RA, Vallee BL. Proc. Natl. Acad. Sci. 1984; 81:5041–5045. [PubMed: 6591178]
39. Britt BM, Peticolas WL. J. Am. Chem. Soc. 1992; 114:5295–5303.
40. Mustafi D, Makinen MW. J. Biol. Chem. 1994; 269:4587–4595. [PubMed: 8308030]
41. Lee HC, Ko YH, Baek SB, Kim DH. Bioorg. Med. Chem. Lett. 1998; 8:3379–3384. [PubMed: 9873738]
42. Auld DS, Holmquist B. Biochem. 1974; 13:4355–4361. [PubMed: 4472022]
43. Geoghegan KF, Galdes A, Martinelli RA, Holmquist B, Auld DS. Biochem. 1983; 22:2255–2262. [PubMed: 6305412]
44. Galdes A, Auld DS, Vallee BL. Biochem. 1983; 22:1888–1893. [PubMed: 6849892]
45. Alex A, Clark T. J. Comput. Chem. 1992; 13(6):704–717.
46. Alvarez-Santos S, Gonzalez-Lafont A, Lluch JM. Can. J. Chem. 1994; 72:2077.
47. Alvarez-Santos S, Gonzalez-Lafont A, Lluch JM, Oliva B, Aviles FX. New J. Chem. 1998:319–325.
48. Kilshtain-Vardi A, Shoham G, Goldblum A. Int. J. Quant. Chem. 2002; 88:87–98.
49. Vardi-Kilshtain A, Shoham G, Goldblum A. Mol. Phys. 2003; 101(17):2715–2724.
50. Banci L, Bertini I, La Penna G. Proteins. 1994; 18:186–197. [PubMed: 8159667]
51. Szeto MWY, Mujika JI, Zurek J, Mulholland AJ, Harvey JN. J. Mole. Struct. (THEOCHEM). 2009; 898:106–114.
52. Klishtain AV, Warshel A. Proteins: Struct., Funct., Bioinfo. 2009; 77 563-560.
53. Xu D, Guo H. J. Am. Chem. Soc. 2009; 131:9780–9788. [PubMed: 19552427]
54. Warshel A, Levitt M. J. Mol. Biol. 1976; 103:227–249. [PubMed: 985660]
55. Senn HM, Thiel W. Angew. Chem. Int. Ed. 2009; 48:1198–1229.
56. Elstner M, Porezag D, Jungnickel G, Elsner J, Haugk M, Frauenheim T, Suhai S, Seigert G. Phys. Rev. 1998; B58:7260–7268.
57. MacKerell AD Jr, Bashford D, Bellott M, Dunbrack RL Jr, Evanseck JD, Field MJ, Fischer S, Gao J, Guo H, Ha S, Joseph-McCarthy D, Kuchnir L, Kuczera K, Lau FTK, Mattos C, Michnick S, Ngo T, Nguyen DT, Prodhom B, Reiher WE III, Roux B, Schlenkrich M, Smith JC, Stote R,

Straub J, Watanabe M, Wiorkiewicz-Kuczera J, Yin D, Karplus M. J. Phys. Chem. B. 1998; 102:3586–3616.

58. Corminboeuf C, Hu P, Tuckerman ME, Zhang Y. J. Am. Chem. Soc. 2006; 128:4530–4531. [PubMed: 16594663]
59. Wu R, Hu P, Wang S, Cao Z, Zhang Y. J. Chem. Theo. Comput. in press.
60. Cui Q, Elstner M, Kaxiras E, Frauenheim T, Karplus M. J. Phys. Chem. B. 2001; 105:569–585.
61. Riccardi D, Schaefer P, Yang Y, Yu H, Ghosh N, Prat-Resina X, Konig P, Li G, Xu D, Guo H, Elstener M, Cui Q. J. Phys. Chem. B. 2006; 110:6458–6469. [PubMed: 16570942]
62. Sattelmeyer KW, Tirado-Rives J, Jorgensen WL. J. Phys. Chem. A. 2006; 110:13551–13559. [PubMed: 17165882]
63. Otte N, Scholten M, Thiel W. J. Phys. Chem. A. 2007; 111:5751–5755. [PubMed: 17385847]
64. Seabra, GdM; Walker, RC.; Elstner, M.; Case, DA.; Roitberg, AE. J. Phys. Chem. A. 2007; 111:5655–5664. [PubMed: 17521173]
65. Elstner M, Cui Q, Munih P, Kaxiras E, Frauenheim T, Karplus M. J. Comput. Chem. 2003; 24:565–581. [PubMed: 12632471]
66. Riccardi D, Cui Q. J. Phys. Chem. A. 2007; 111:5703–5711. [PubMed: 17506534]
67. Riccardi D, Konig P, Guo H, Cui Q. Biochem. 2008; 47:2369–2378. [PubMed: 18247480]
68. Xu D, Zhou Y, Xie D, Guo H. J. Med. Chem. 2005; 48:6679–6689. [PubMed: 16220984]
69. Xu D, Xie D, Guo H. J. Biol. Chem. 2006; 281:8740–8747. [PubMed: 16423823]
70. Xu D, Guo H, Cui Q. J. Phys. Chem. A. 2007; 111:5630–5636. [PubMed: 17388313]
71. Xu D, Guo H, Cui Q. J. Am. Chem. Soc. 2007; 129:10814. [PubMed: 17691780]
72. Wang C, Guo H. J. Phys. Chem. B. 2007; 111:9986–9992. [PubMed: 17663582]
73. Simona F, Magistrato A, Dal Peraro M, Cavalli A, Vila AJ, Carloni P. J. Biol. Chem. 2009; 284:28164. [PubMed: 19671702]
74. Jorgensen WL, Chandrasekhar J, Madura JD, Impey RW, Klein ML. J. Chem. Phys. 1983; 79:926–935.
75. Brooks CL III, Brunger A, Karplus M. Biopoly. 1985; 24:843.
76. Field MJ, Bash PA, Karplus M. J. Comput. Chem. 1990; 11:700–733.
77. Steinbach PJ, Brooks BR. J. Comput. Chem. 1994; 15:667.
78. Brooks BR, Bruccoleri RE, Olafson BD, States DJ, Swaminathan S, Karplus M. J. Comput. Chem. 1983; 4:187–217.
79. Ryckaert JP, Ciccotti G, Berendsen HJ. J. Comput. Phys. 1977; 23:327–341.
80. Torrie GM, Valleau JP. J. Comput. Phys. 1977; 23:187–199.
81. Kumar S, Bouzida D, Swendsen RH, Kollman PA, Rosenberg JM. J. Comput. Chem. 1992; 13:1011–1021.
82. Gonzalez C, Schlegel HB. J. Phys. Chem. 1990; 94:5523.
83. Becke AD. J. Chem. Phys. 1993; 98:5648–5652.
84. Lee C, Yang W, Parr RG. Phys. Rev. B. 1988; 37:785–789.
85. Frisch, MJ.; Trucks, GW.; Schlegel, HB.; Scuseria, GE.; Robb, MA.; Cheeseman, JR.; Montgomery, JA.; Vreven, T., Jr; Kudin, KN.; Burant, JC.; Millam, JM.; Iyengar, SS.; Tomasi, J.; Barone, V.; Mennucci, B.; Cossi, M.; Scalmani, G.; Rega, N.; Petersson, GA.; Nakatsuji, H.; Hada, M.; Ehara, M.; Toyota, K.; Fukuda, R.; Hasegawa, J.; Ishida, M.; Nakajima, T.; Honda, Y.; Kitao, O.; Nakai, H.; Klene, M.; Li, X.; Knox, JE.; Hratchian, HP.; Cross, JB.; Adamo, C.; Jaramillo, J.; Gomperts, R.; Stratmann, RE.; Yazyev, O.; Austin, AJ.; Cammi, R.; Pomelli, C.; Ochterski, JW.; Ayala, PY.; Morokuma, K.; Voth, GV.; Salvador, P.; Dannenberg, JJ.; Zakrzewski, VG.; Dapprich, S.; Daniels, AD.; Strain, MC.; Farkas, O.; Malick, DK.; Rabuck, AD.; Raghavachari, K.; Foresman, JB.; Ortiz, JV.; Cui, Q.; Baboul, AG.; Clifford, S.; Cioslowski, J.; Stefanov, BB.; Liu, G.; Liashenko, A.; Piskorz, P.; Komaromi, I.; Martin, RL.; Fox, DJ.; Keith, T.; Al-Laham, MA.; Peng, CY.; Nanayakkara, A.; Challacombe, M.; Gill, PMW.; Johnson, B.; Chen, W.; Wong, MW.; Gonzalez, C.; Pople, JA. Gaussian 03, Revision A.1. Pittsburgh, PA: Gaussian, Inc.; 2003.
86. Quiocho FA, Lipscomb WM. Adv. Protein Chem. 1971; 25:1–78. [PubMed: 4946703]

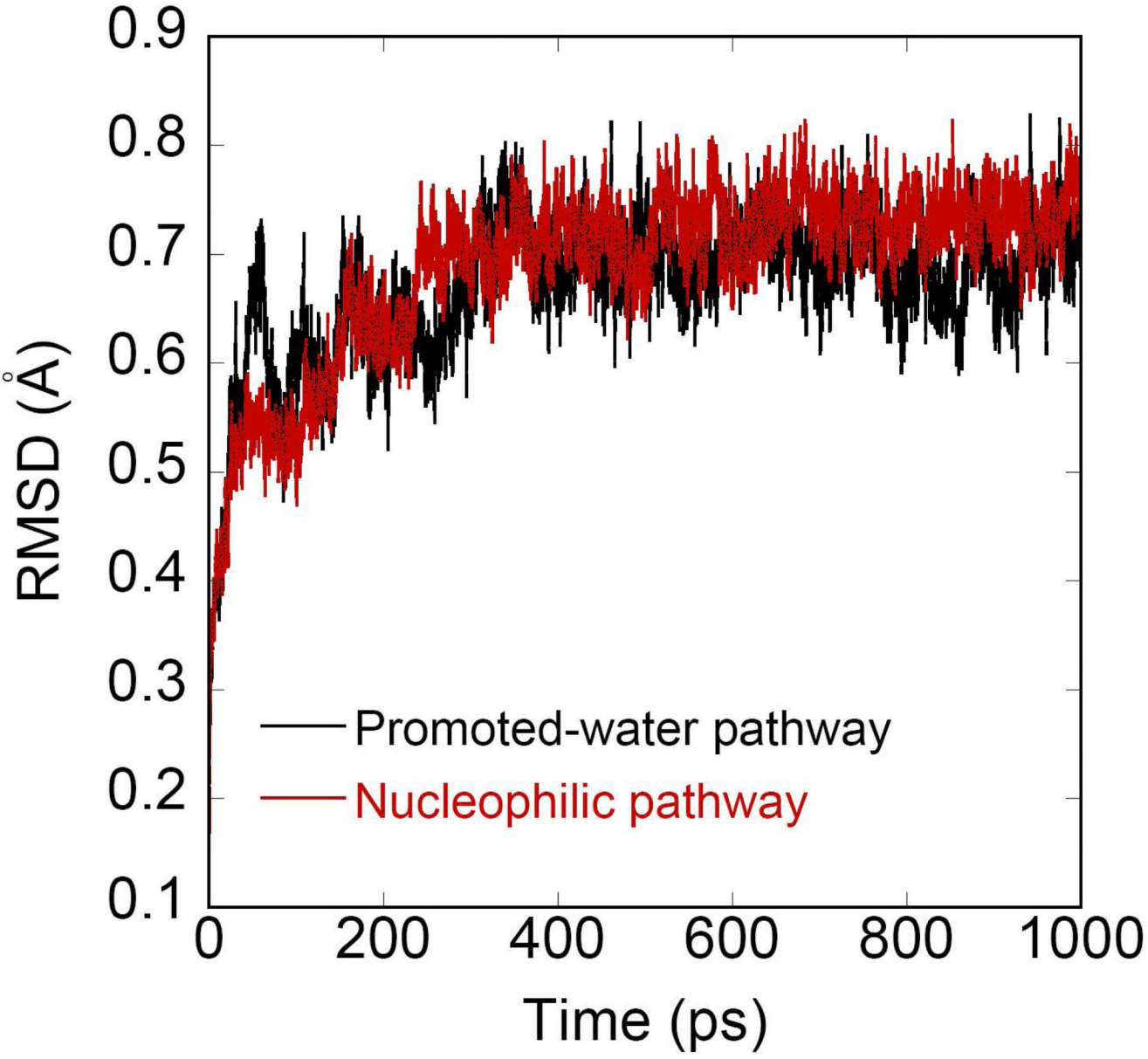

Fig. 1.
RMSD for the enzyme-substrate complex for the promoted-water pathway (black) and nucleophilic pathway (red).

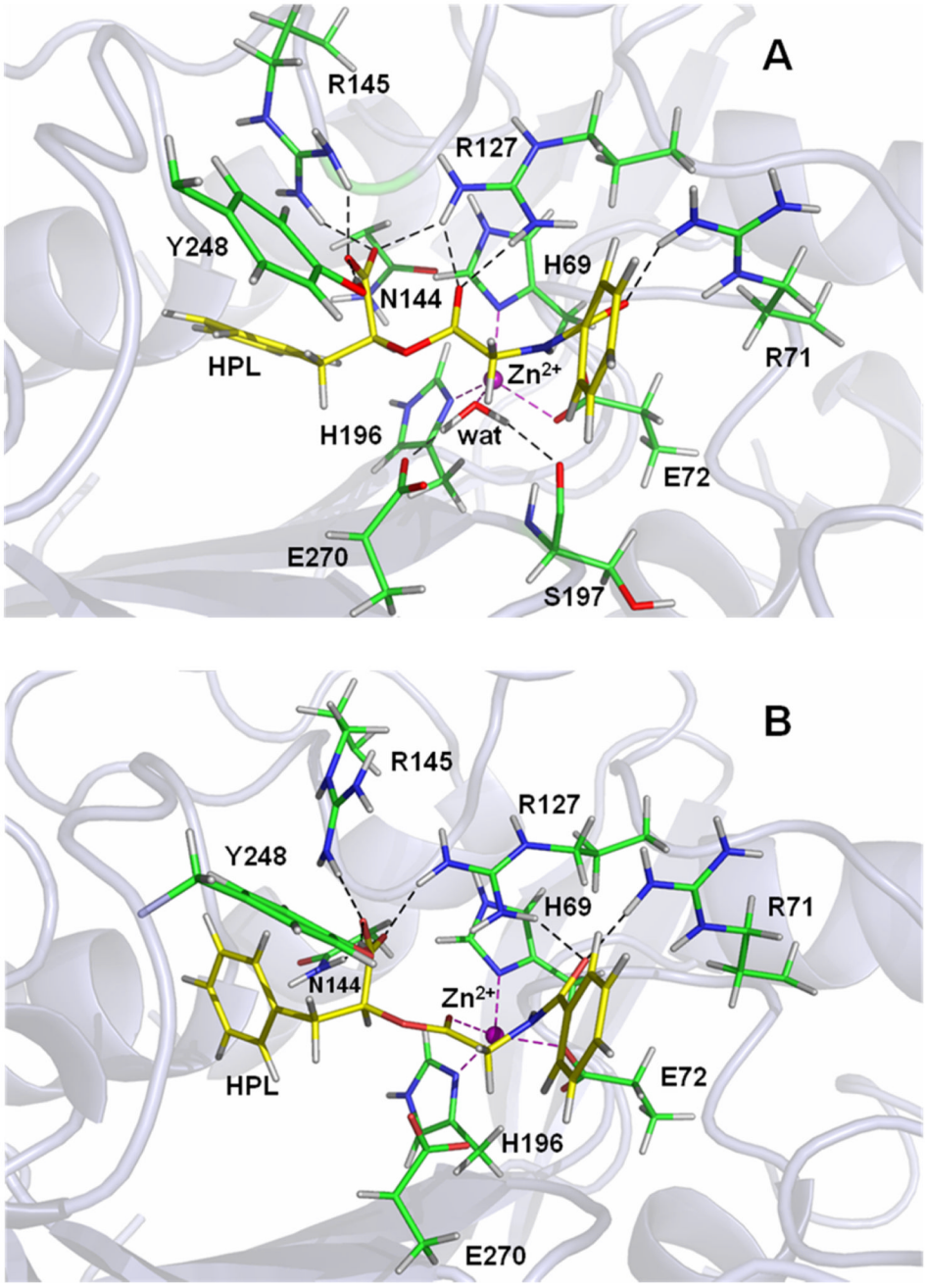

Fig. 2.

Snapshots of enzyme-substrate complexes for the promoted-water mechanism (A) and nucleophilic pathway (B) obtained from QM/MM MD simulations. The substrate is coded yellow. Black dashed lines represent hydrogen bonds, while purple dashed lines metal-ligand bonds.

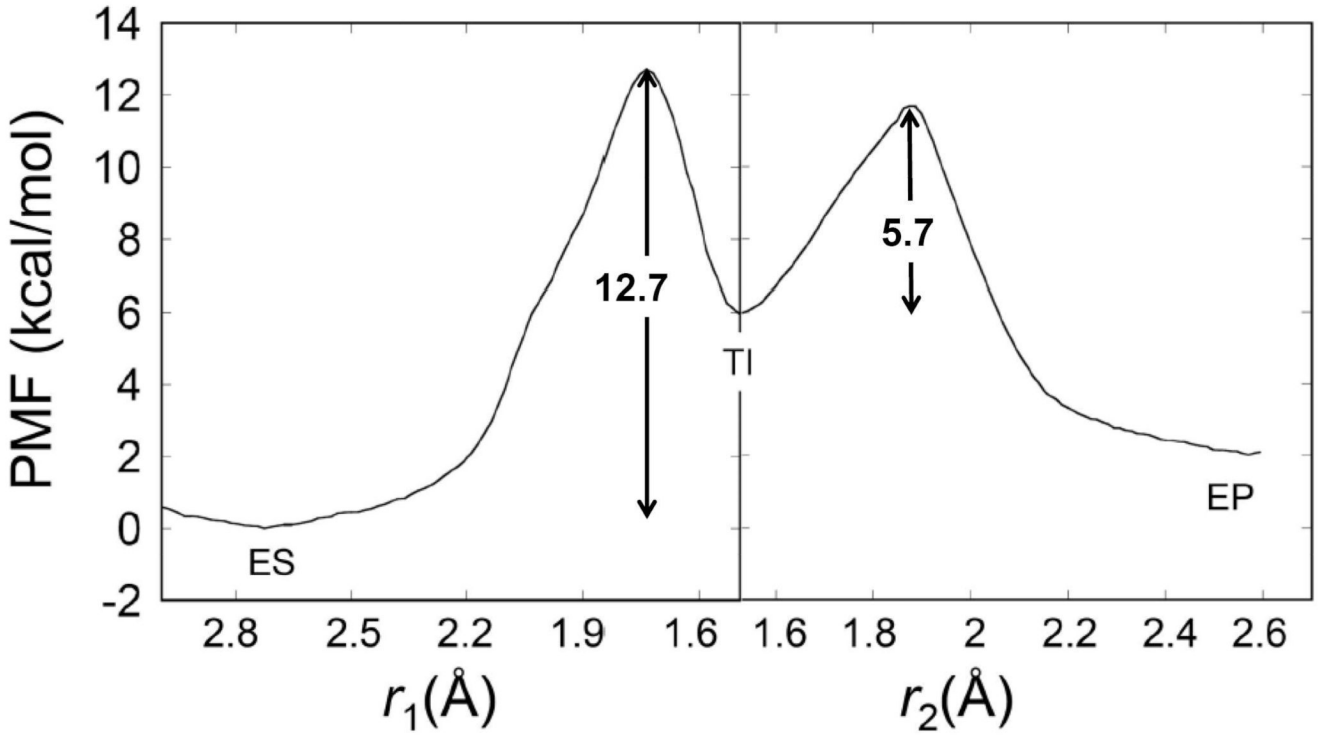

Fig. 3.
Potentials of mean force (PMFs) for the CPA catalyzed hydrolysis of the ester (HPL) via the promoted-water mechanism.

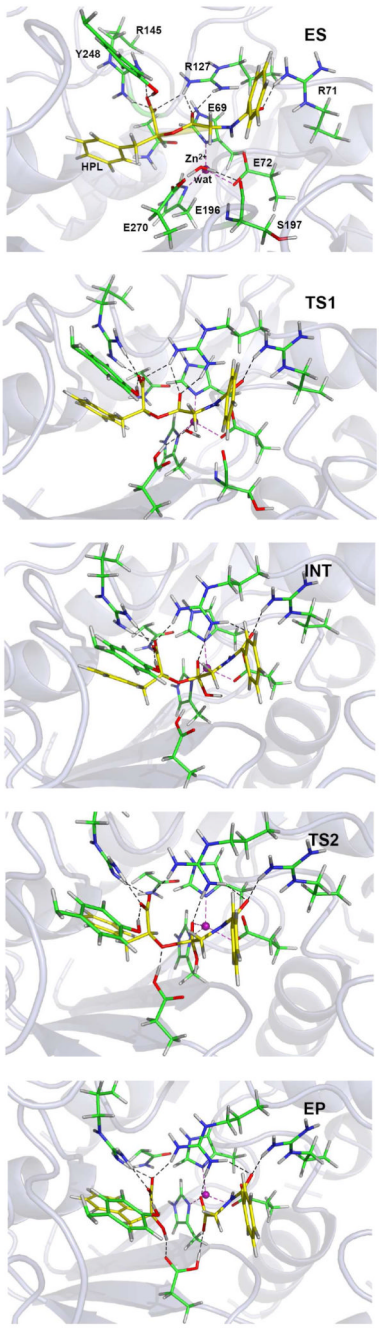

Fig. 4.
Stationary point structures for the promoted-water pathway obtained by SCC-DFTB/MM reaction path calculations.

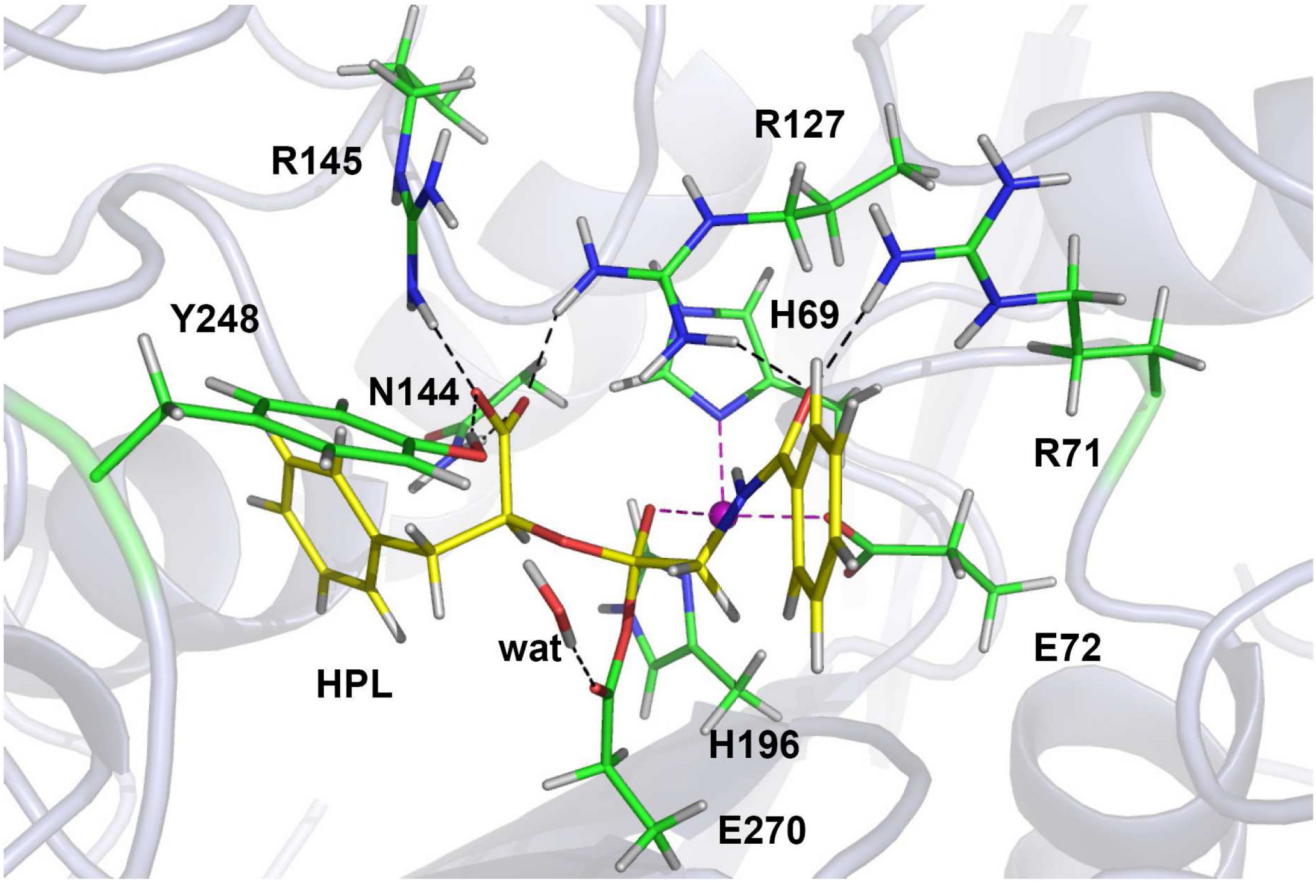

Fig. 5.
Snapshots of the acyl-enzyme intermediate complex for the nucleophilic pathway obtained from QM/MM MD simulations. The substrate is coded yellow. Black dashed lines represent hydrogen bonds, while purple dashed lines metal-ligand bonds.

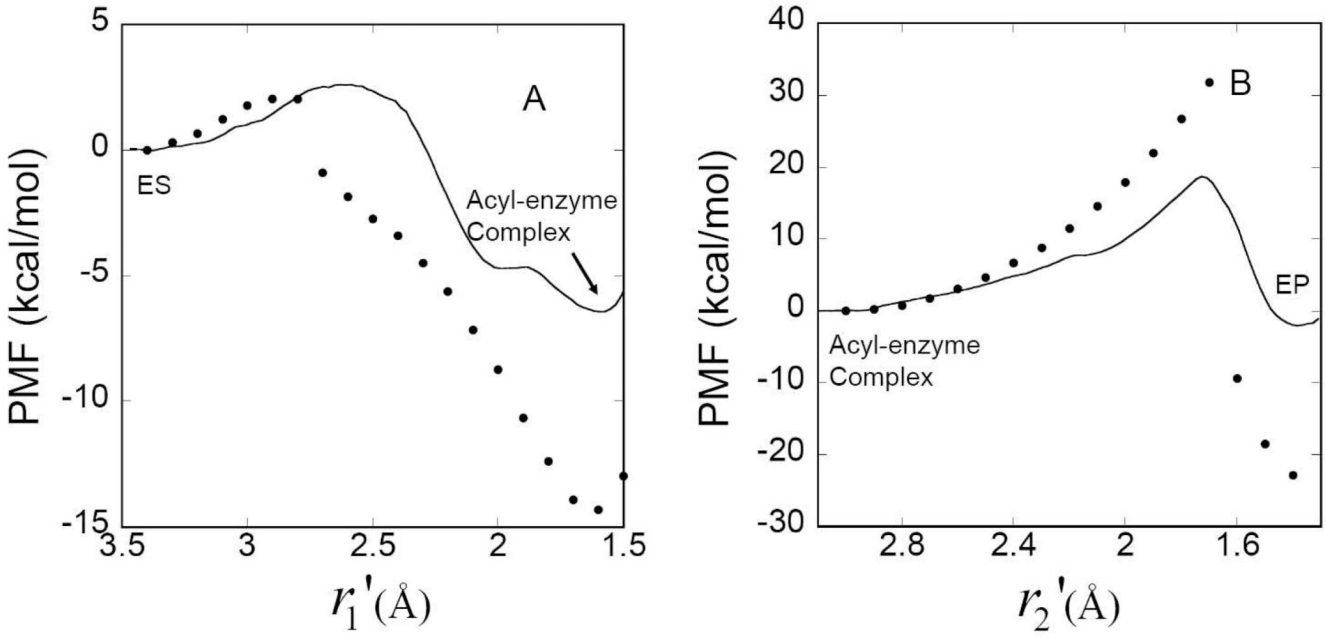

Fig. 6.

Potentials of mean force (PMFs) for the CPA catalyzed hydrolysis of the ester (HPL) via the nucleophilic pathway. The acylation and deacylation steps are depicted in panels A and B. Single-point B3LYP/MM//SCC-DFTB/MM results (filled circles) are also shown for comparison.

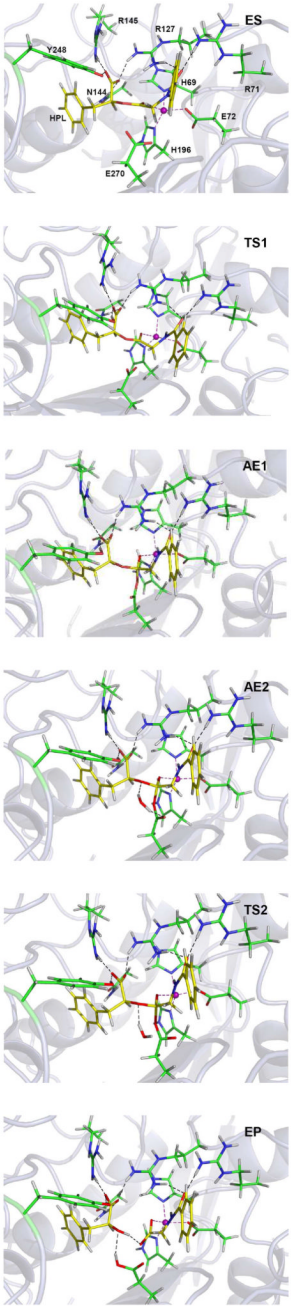

Fig. 7.
Stationary point structures for the nucleophilic pathway obtained by SCC-DFTB/MM reaction path calculations.

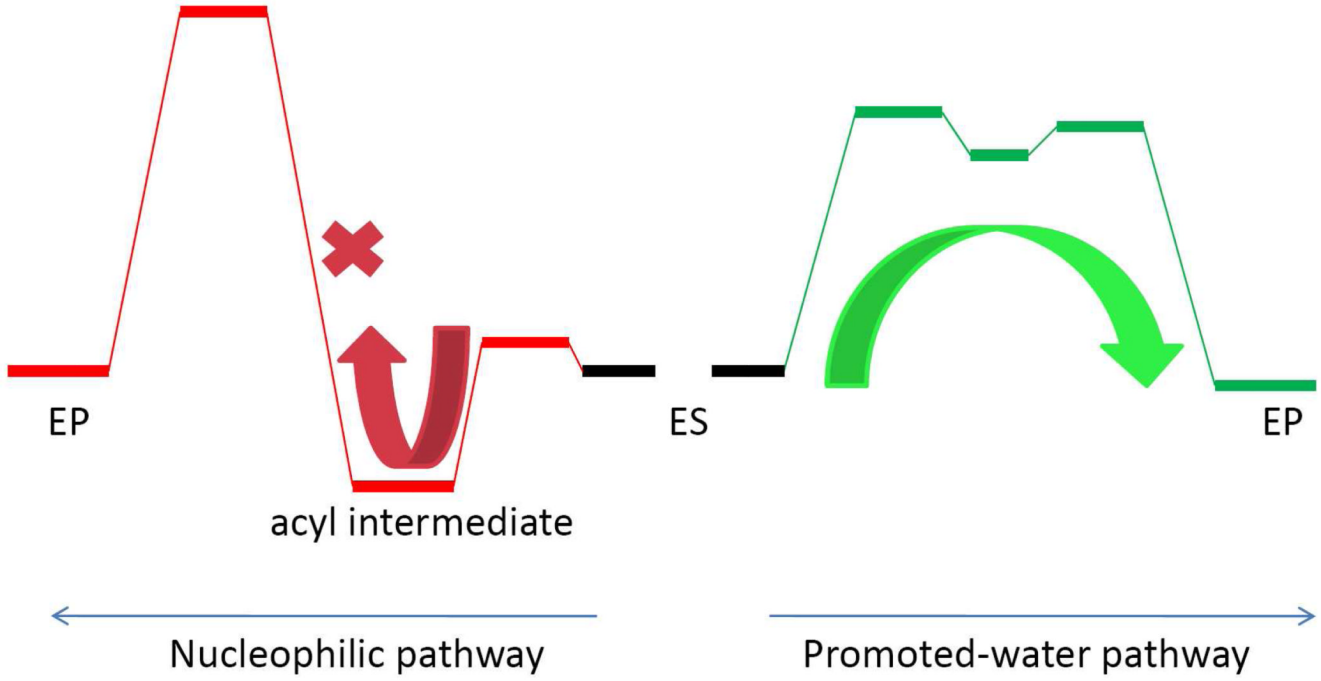

Fig. 8.
Schematic depiction of the two pathways in the CPA catalyzed esterolysis.

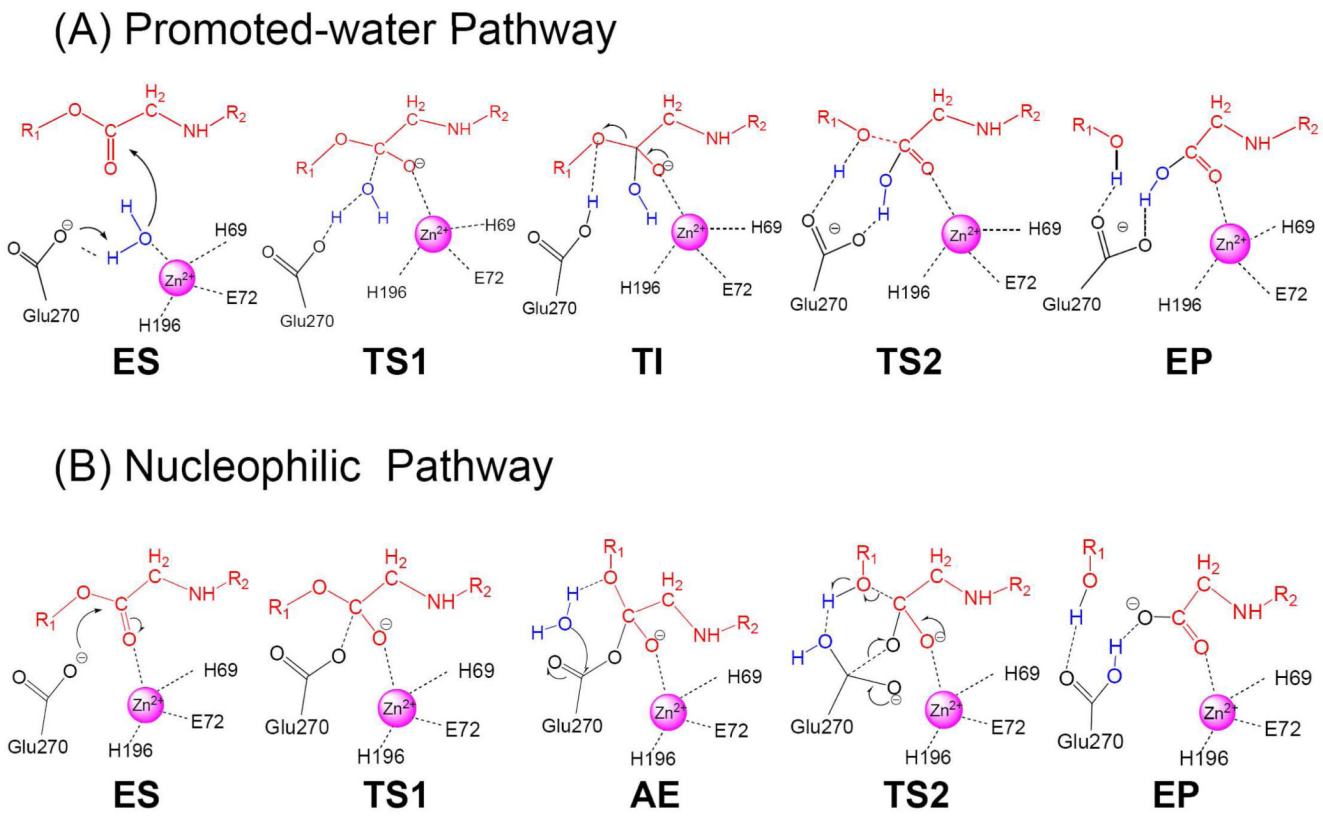

Scheme 1.
Two possible reaction pathways, promoted-water pathway (A) and nucleophilic pathway (B), for ester hydrolysis catalyzed by carboxypeptidase A.

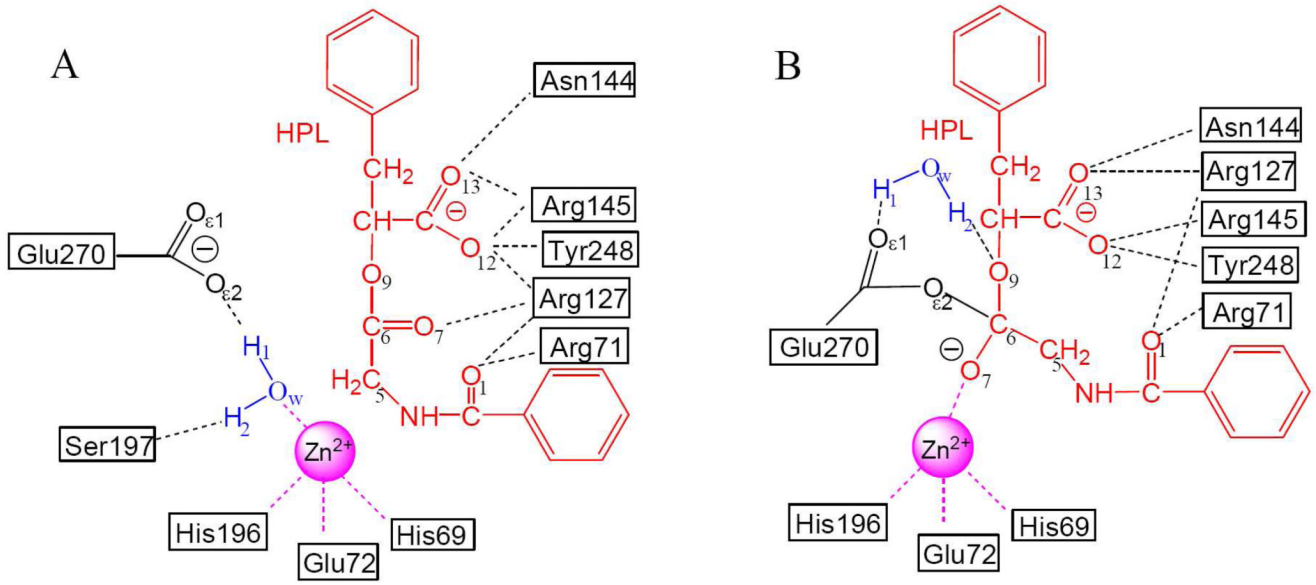

Scheme 2.

Atom definition and corresponding interactions between the ester substrate (HPL) and active-site residues. Panel A: the ES complex for the promoted-water pathway. Panel B: the acyl-enzyme complex for the nucleophilic pathway.

Table 1

Selected geometric parameters of stationary points for the promoted-water pathway obtained at the SCC-DFTB/MM level of theory, and from QM/MM MD simulations.

Distance (Å)	QM/MM Reaction Path					QM/MM MD ES
	ES	TS1	TI	TS2	EP	
$O_w \cdots C_6$	3.19	1.78	1.49	1.37	1.30	3.39±0.24
$H_1 \cdots O_{\varepsilon 2}$(E270)	1.24	1.03	1.00	1.10	1.81	1.45±0.13
$H_1 \cdots O_w$	1.19	1.63	1.81	2.43	2.83	-
$H_2 \cdots$O(S197)	1.86	1.80	1.79	2.89	3.57	1.75±0.19
$Zn \cdots N_{\delta 1}$(H69)	2.00	2.00	2.00	1.97	1.99	1.99±0.11
$Zn \cdots O_{\varepsilon 2}$(E72)	2.14	2.12	2.14	2.11	2.10	2.04±0.05
$Zn \cdots N_{\delta 1}$(H196)	1.99	2.00	2.00	1.97	1.98	1.97±0.03
$O_9 \cdots O_{\varepsilon 1}$(E270)	4.07	3.08	2.76	2.45	2.89	3.40±0.33
$O_w \cdots Zn$	2.03	2.17	2.89	2.92	3.14	2.05±0.09
$Zn \cdots O_7$	3.90	2.87	2.15	2.14	2.15	4.23±0.15
$O_7 \cdots H_{21}$(R127)	1.84	1.81	1.78	1.88	1.85	1.78±0.28
$O_7 \cdots H_{11}$(R127)	2.04	3.08	3.12	3.25	3.37	1.95±0.31
$O_{12} \cdots H_{11}$(R127)	2.31	1.88	1.86	1.82	1.83	2.50±0.21
$O_{13} \cdots H_{22}$(N144)	2.74	2.67	2.68	2.78	2.87	2.72±0.31
$O_{12} \cdots H_{21}$(R145)	1.69	1.71	1.72	1.71	1.70	1.57±0.16
$O_{13} \cdots H_{11}$(R145)	1.64	1.65	1.65	1.65	1.65	1.66±0.21
$C_5 \cdots C_6$	1.51	1.53	1.55	1.53	1.53	-
$C_6 \cdots O_7$	1.23	1.32	1.39	1.30	1.26	-
$C_6 \cdots O_9$	1.36	1.43	1.41	1.90	3.19	-
$H_1 \cdots O_9$	2.63	2.48	2.20	1.40	1.00	-
$O_{12} \cdots H_{\eta}$(Y248)	1.66	1.65	1.64	1.64	1.64	1.70±0.12
$O_1 \cdots H_{12}$(R71)	1.75	1.78	1.79	1.77	1.74	1.60±0.19
$O_1 \cdots H_{22}$(R127)	2.15	2.16	2.19	2.18	2.22	2.03±0.13

J Phys Chem B. Author manuscript; available in PMC 2011 July 22.

Table 2

Energetics (kcal/mol) of the truncated active-site model for the promoted-water pathway.

Methods	ES	TS1	TI1	TI2	TS3	EP
Energy (B3LYP/6-31G(d))	0.0	24.36	11.47	−0.28	9.23	−34.05
Free energy (B3LYP/6-31G(d))	0.0	24.34	11.49	−0.31	9.28	−34.05
PCM (B3LYP/6-31G(d) w/ε=80)	0.0	17.79	9.21	−2.91	5.08	−25.04
PCM (B3LYP/6-31G(d) w/ε=5)	0.0	22.60	10.38	−0.02	8.27	−28.59
Energy (B3LYP/6-31+G(d,p)// B3LYP/6-31G(d))	0.0	27.24	15.87	2.42	10.77	−32.06
Energy (SCC-DFTB// B3LYP/6-31G(d))	0.0	17.61	2.09	−5.03	3.96	−28.27

Table 3

Selected geometric parameters of stationary points for the nucleophilic pathway obtained at the SCC-DFTB/MM level of theory and from QM/MM MD simulations.

Distance (Å)	QM/MM Reaction Path						QM/MM MD ES	QM/MM MD AE2
	ES	TS1	AE1	AE2	TS2	EP		
$C_5\cdots C_6$	1.46	1.50	1.55	1.53	1.54	1.45	1.45±0.08	1.54±0.03
$C_6\cdots O_7$	1.34	1.34	1.49	1.47	1.35	1.32	1.33±0.11	1.50±0.09
$C_6\cdots O_9$	1.26	1.26	1.37	1.34	1.49	3.06	1.28±0.09	1.38±0.04
$C_6\cdots O_{\varepsilon 2}$(E270)	3.20	2.59	1.42	1.57	1.54	1.24	3.32±0.17	1.40±0.06
$O_w\cdots C_\delta$ (E270)	-	-	-	3.20	1.74	1.32	-	3.28±0.35
$H_2\cdots O_9$	-	-	-	1.93	1.73	0.99	-	1.98±0.34
$H_2\cdots O_w$	-	-	-	0.98	1.00	2.54	-	0.99±0.03
$H_1\cdots O_{\varepsilon 1}$(E270)	-	-	-	1.80	2.25	2.30		1.83±0.28
$O_{\varepsilon 2}\cdots C_\delta$ (E270)	-	-	-	1.37	1.49	2.66	-	-
$Zn\cdots N_{\delta 1}$(H69)	2.00	2.00	2.02	2.02	2.02	1.99	2.01±0.04	2.01±0.03
$Zn\cdots O_{\varepsilon 2}$(E72)	2.07	2.08	2.10	2.10	2.11	2.10	2.10±0.06	2.11±0.02
$Zn\cdots N_{\delta 1}$(H196)	1.95	1.95	1.98	1.98	1.97	1.96	1.96±0.03	1.98±0.03
$Zn\cdots O_7$	2.18	2.16	2.05	2.05	2.05	2.06	2.17±0.08	2.04±0.04
$O_7\cdots H_{21}$(R127)	2.76	2.79	2.61	2.72	2.81	2.51	2.75±0.25	2.58±0.13
$O_7\cdots H_{11}$(R127)	3.90	3.90	4.00	4.11	4.08	3.92	3.91±0.16	3.99±0.16
$O_{13}\cdots H_{11}$(R127)	1.84	1.83	1.82	1.82	1.82	1.80	1.84±0.14	1.86±0.24
$O_{13}\cdots H_{22}$(N144)	1.83	1.84	1.82	1.82	1.83	1.87	1.82±0.20	1.83±0.15
$O_{12}\cdots H_{21}$(R145)	1.79	1.79	1.77	1.76	1.81	1.75	1.79±0.13	1.79±0.13
$O_{12}\cdots H_{11}$(R127)	2.67	2.69	2.69	2.73	2.76	2.88	2.69±0.18	2.68±0.17
$O_{12}\cdots H_\eta$(Y248)	1.69	1.68	1.68	1.70	1.69	1.72	1.69±0.05	1.69±0.04
$O_7\cdots H_\eta$(Y248)	-	-	-	-	-	-	4.56±0.41	-
$O_1\cdots H_{12}$(R71)	1.71	1.73	1.72	1.70	1.70	1.72	1.74±0.23	1.73±0.16
$O_1\cdots H_{22}$(R127)	1.99	1.98	1.93	1.90	1.89	1.97	1.98±0.16	1.92±0.05

J Phys Chem B. Author manuscript; available in PMC 2011 July 22.

Table 4

Energetics (kcal/mol) of the truncated active-site model for the nucleophilic pathway.

Methods	ES	TS1	AE1	AE2	TS2	EP
Energy (B3LYP/6-31G(d, p))	0.0	16.61	11.82	0	35.02	−51.34
Free energy (B3LYP/6-31G(d, p))	0.0	15.43	10.57	0	36.73	−59.63
PCM (B3LYP/6-31G(d, p) w/ε=80)	0.0	8.39	2.08	0	31.72	−49.53
PCM (B3LYP/6-31G(d, p) w/−=5)	0.0	11.00	1.91	0	33.80	−46.70
Energy (B3LYP/6-31++G(d, p)// B3LYP/6-31G(d, p))	0.0	19.30	14.45	0	36.00	−52.39
Energy (SCC-DFTB// B3LYP/6-31G(d, p))	0.0	8.18	−2.53	0	36.75	−50.34